Ultrafast Solvation Processes in Polar Liquids Probed with Large Organic Molecules

C. J. Bardeen,† S. J. Rosenthal,‡ and C. V. Shank*

Department of Chemistry, University of California, Berkeley Berkeley, California 94720, and Materials Sciences Division, Lawrence Berkeley National Laboratory, 1 Cyclotron Road Berkeley, California 94720

Received: June 15, 1999; In Final Form: October 11, 1999

Several optical techniques are used to characterize the ultrafast solvation dynamics of two structurally different molecules, LD690 and LDS750. Linear absorption, fluorescence, resonance Raman, and time-resolved four-wave mixing experiments have been performed on both molecules in a variety of solvents. The combination of different experiments is necessary to characterize the femtosecond dynamics. We find that both molecules exhibit very fast dephasing, due to sub-100 fs decays of the solvation correlation function $M(t)$. The LD690 data is analyzed in depth, using a multimode oscillator model to treat both intramolecular vibrations and the solvent coordinates. The dynamics are solvent-dependent, but this dependence cannot be explained in a straightforward manner using quantities such as inertial solvent rotational motion or a simple dielectric continuum response. Various aspects of the spectroscopy, both linear and nonlinear, provide clues that the dynamics are influenced by molecular-level interactions that are not taken into account by theories that only consider bulk solvent properties.

Introduction

The dynamics of the solvent−solute interaction are important in determining chemical reaction rates in liquid solution. The response of the solvent molecules to a change in the solute's charge distribution is known as solvation and plays a key role in determining the microscopic friction of reaction rate theories. If linear response theory holds, the solvent response to the rearrangement of charge that takes place during a chemical reaction will be the same as that to any other process that results in a charge redistribution. In particular, absorption of a photon leads to an electronically excited state whose charge distribution is out of equilibrium with its solvent environment. The subsequent solvent relaxation, which results in optical dephasing and a dynamic Stokes shift of the fluorescence, reflects the solvation of the newly created charge distribution. In this way, optical spectroscopy provides a window onto microscopic solvation dynamics.

The absorption line shape contains information about dynamics, but in the condensed phase it is often featureless and uninformative, and the underlying processes that give rise to it are not obvious. For instance, the width of an absorption spectrum could result from a large number of slowly interconverting sites with different energies (inhomogeneous broadening), from fast processes that randomize the energy (homogeneous broadening), from unresolved vibrational progressions, or from a combination of all three.

To sort out these possibilities, it is necessary to employ nonlinear optical techniques in either the time or frequency domains.[1] Frequency domain techniques include resonance Raman[2] and resonant four-wave mixing and scattering spectroscopies.[3] Time domain methods include transient absorption[4] and hole burning,[5] time-resolved fluorescence,[6] and time-resolved four-wave mixing spectroscopies such as the transient grating[7] and photon echo.[8−11] For dynamics taking place on time scales greater than a few hundred femtoseconds, the time-resolved Stokes shift method provides the most direct and easily interpretable data.[12] Using this method to probe solvation at shorter times is problematic, both because the usual approximations of complete vibrational relaxation and an unchanging fluorescence spectrum may not be valid and because there may be significant spectral overlap between the exciting laser pulse and the fluorescence at very early times. In the linear response limit, the electronic dephasing of the optical transition is directly related to the dynamic Stokes shift and provides a measure of the femtosecond dynamics of solvation.[13] This dephasing can be measured using the photon echo, which uses a sequence of pulses to cancel out the effects of the slow (inhomogeneous) variables on the observed signal, revealing the fast dynamics that determine the optical dephasing. Two- and three-pulse photon echoes have proved valuable in probing very fast solvation dynamics that are difficult to observe using the time-resolved fluorescence technique. Using the three-pulse photon echo (3PPE), the dynamics of several dyes in various solvents have been mapped out.[14−17] The results of these measurements have yielded varying estimates of the shortest time events in solvation, although there is general agreement that the initial solvent response occurs on a time scale of 100 fs or less. This temporal region is of great interest since it is inaccessible to most other techniques and is postulated to be the domain of inertial solvation,[18,19] where the response is dominated by the inertial motion of individual solvent molecules, which later gives way to the collective motion that determines the bulk dielectric function.

In this paper we present a set of measurements, both frequency and time-resolved, in an attempt to provide a self-consistent picture of the ultrafast solvation dynamics for one molecule in particular, LD690 (Oxazine 4), in a variety of solvents. We compare these results to those obtained from a structurally dissimilar molecule that absorbs in the same range,

† Present address: Department of Chemistry, University of Illinois, 600 S. Mathews Ave, Urbana, Illinois 61801.
‡ Present address: Department of Chemistry, Vanderbilt University, Nashville, Tennessee 37235.

10.1021/jp991974k CCC: $18.00
Published on Web 11/19/1999

LDS750, to clarify how differences in solute can affect these measurements. By analyzing linear absorption and fluorescence spectra, resonance Raman spectra, and time-integrated 3PPE data, we show that the ultrafast time-domain signals alone are insufficient to conclusively determine the time scale of the solvation correlation function. It is necessary to combine several different experimental methods to provide constraints for models of the solute−solvent complex and separate the intra- and intermolecular contributions to the observed signals. After taking the intramolecular contribution to the femtosecond dynamics of LD690 into account, we find that the variation of the ultrafast solvation dynamics and Stokes shift with solvent is not easily explained by models based on either simple inertial solvent dipole reorientation[18−20] or bulk solvent dielectric response.[21−23] Our data suggests that specific molecular interactions play at least some role in the solvation of LD690 and LDS750.

Experiment

The dyes and solvents are used as received from the manufacturers without further purification. All absorption measurements are done using an Aviv 14DS spectrometer, and the only correction to the data is background subtraction. The fluorescence data are collected on a home-built apparatus, using the 514.5 nm line of an argon ion laser to excite the sample and detecting the fluorescence perpendicular to the excitation beam with a scanning monochromator and a PMT. Experiments on a multiwavelength fluorometer have shown that the shape of the fluorescence spectrum is independent of the excitation wavelength. The resonance Raman data are obtained similarly, using a 514.5 nm argon ion laser light to excite the sample and collecting the scattered light perpendicular to the beam, which is directed into a double monochromator and imaged onto a cooled CCD array. The workup of both the fluorescence and resonant Raman data involves correcting for the sensitivity of the detectors and for the self-absorption of the sample.

The experimental setup for the 3PPE measurements has been described before[15] and will only be outlined briefly here. Pulses from a colliding pulse mode-locked dye laser are amplified at an 8 kHz repetition rate and used to generate continuum in a single mode optical fiber, which is then reamplified in a broadband dye amplifier. The output pulses are centered at 620 nm and have a typical duration of about 12 fs. A typical power spectrum, along with the absorption spectra of LD690 and LDS750 in methanol, is shown in Figure 1. At the experiment the beam is split into three pulses, which can be delayed with respect to one another and which are crossed in the sample. The scattered signal in the $-\mathbf{k}_1 + \mathbf{k}_2 + \mathbf{k}_3$ direction is directed into a PMT, and lock-in detection is used to improve the signal-to-noise ratio. The pulse energies are adjusted so that the detected signal varies as the cube of the pulse intensity, as expected in the perturbation (small pulse area) limit. The samples are either a flowing 70 μm thick jet of an approximately 10^{-4} M dye solution or a 100 μm path length flow cell containing the dye solution. In both cases the flow rate is sufficiently rapid to guarantee complete replacement of the sample between laser shots. The extra dispersion from the front wall of the cell is precompensated for, ensuring that the pulse is short at the sample itself. For all experiments the transmittance of the sample is l/e or greater.

One can think of the 3PPE excitation sequence in the following way: the first field interaction ($\mathbf{k}_1$) excites a polarization in the sample, which rapidly decays until the second field interaction ($\mathbf{k}_2$) converts it into a population after a delay t_{12}.

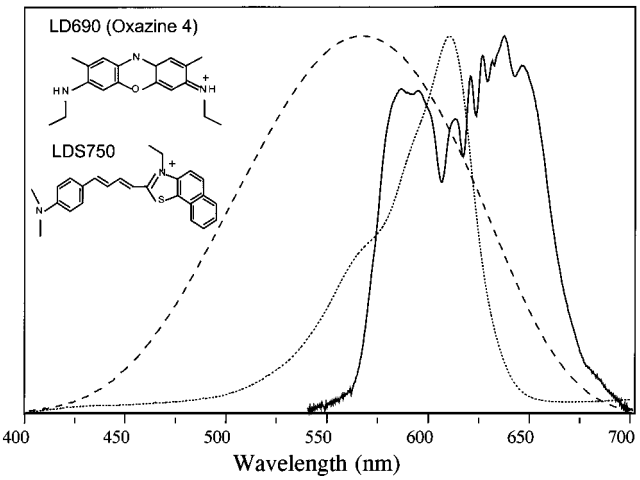

Figure 1. Absorption spectra of LD690 (short dashed line) and LDS750 (long dashed line) in methanol, along with $|E(\lambda)|$ (solid line).

Each molecule in this population has a phase term that depends on its detuning from the laser frequency due to the inhomogeneous distribution. The molecules evolve for a time, subject to relaxation and spectral diffusion processes, which result in a randomizing of the inhomogeneous phase term. Finally, a third pulse, delayed by an amount t_{13} with respect to the first pulse, interacts with this population to generate a second polarization which radiates into the $-\mathbf{k}_1 + \mathbf{k}_2 + \mathbf{k}_3$ direction. If the molecules have not forgotten their initial phase terms, the initial detuning phases cancel each other out and only the true dephasing is observed. In this case the t_{12} signal dependence reflects only the fast processes that occurred between pulses 1 and 2, since the slow processes have been rephased during the echo process. If significant spectral diffusion has occurred during t_{13}, the t_{12} signal reflects both the fast and slow components and appears to decay more quickly. In a loose sense, the t_{12} signal is related to the Fourier transform of the part of the spectral line shape that has been sampled by a molecule during time t_{13}. It is important to note that the fast dephasing during t_{12} and the spectral diffusion during t_{13} can be due to both intra- and intermolecular processes.

Ideally, the laser pulse is much shorter than the dynamics, and the t_{12} decay can be directly observed. For the simple case of Markovian (T_2) dephasing, the dephasing rate can be extracted from the slope of the echo signal as a function of t_{12} for $t_{12} > 0$. Alternatively, if the dephasing occurs within the time resolution of the experiment, the spectral diffusion parameters can be extracted from the temporal shift of the t_{12} signal as a function of t_{13}.[24] Joo et al. have shown that, for $t_{13} > 100$ fs, the 3PPE peak shift directly reflects the solvation correlation function $M(t)$.[11] For smaller delays, the situation is more complicated and the detailed pulse shape must be taken into account.[25] To determine the absolute peak shift, one needs to measure the signal in two directions simultaneously, which we were unable to do due to experimental limitations. Thus, we analyze the shape of our 3PPE signals, both as a function of t_{12} and t_{13}. We take advantage of the fact that if one sets t_{12} to a value shorter than the dephasing time (so that there is still some observable signal) but on the order of or larger than the correlation time, the t_{13} scan with $t_{13} > t_{12}$ indirectly reflects the actual decay of the correlation function. This is the same effect that gives rise to the echo peak shift, in which the zero shift of the t_{12} signal peak is measured as a function of third pulse delay t_{13}. This temporal shift in the t_{12} signal manifests itself as a decay during t_{13} if we sit at a given t_{12} and scan t_{13}.

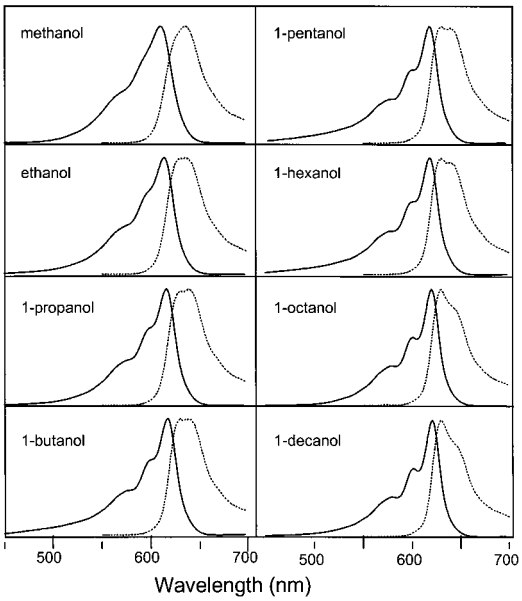

Figure 2. Absorption (solid lines) and fluorescence (dashed lines) of LD690 in the *n*-alcohols.

Finally, the relative timing of the three pulses is very important if intramolecular vibrational modes also influence the signal, and it is possible to cancel out the contribution of at least one vibration by timing the third pulse to arrive at an integer period of that vibration.[26,27] This mode suppression technique is utilized for the experiments on LD690, where the signal is strongly modulated by a vibrational mode at 586 cm^{-1} (corresponding to a period of about 60 fs) and thus t_{13} was set to a multiple of 60 fs. LDS750, on the other hand, has many vibrational modes strongly coupled to the optical transition, and mode suppression is not effective.

Results

A. Frequency Domain Measurements. Figure 2 shows the combined absorption/fluorescence spectra for LD690 in a series of *n*-alcohols. The absorption shape in all solvents in consistent with a single absorbing species with a well-defined vibronic progression. The fluorescence spectra, on the other hand, show a pronounced double-peaked structure in all *n*-alcohols larger than methanol. Moreover, the balance between the two peaks shifts as we go to longer chain (and smaller dielectric constant) alcohols. This double-peaked spectral behavior has been observed before in the absorption spectra of similar molecules in hydrogen bonding solvents and is attributed to the existence of distinct solute−solvent complexes.[28] The absorption redshift and the lack of a significant shift in the fluorescence are both consistent with electronic structure calculations that show that LD690's S_0 ground state is only weakly polar, and the S_1 state is even less polar.[29] The polar ground state increases in energy as the dielectric strength of the solvent decreases, while the excited state does not shift as much, leading to the absorption red shift. Since the S_1 state is not very polar, there is no strongly energetically favored solvent configuration around it, which allows two isomers to coexist and contribute to the fluorescence spectrum. The isomer that fluoresces at higher energy probably corresponds to the less polar species and as the solvent becomes less polar the equilibrium shifts toward this species. This explains the increase in the relative height of the high-energy fluorescence peak as the alcohol chain length is increased.

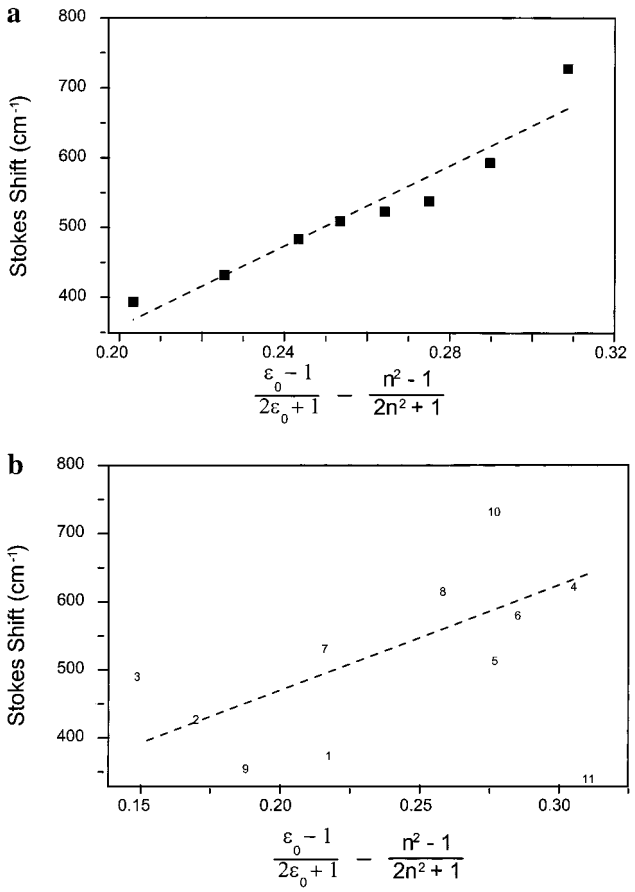

Figure 3. (a) Plot of the Stokes shift of LD690 in *n*-alcohols (n = 1−6, 8, 10), measured as the distance between the centroids of the spectral peaks at their full-width at three-quarters maximum, versus the strength of the solvent dielectric reaction field. The alcohol chain length increases as the Stokes shift decreases. (b) Plot of the Stokes shift of LD690 in various solvents (1 = CH_2Cl_2, 2 = CH_2Br_2, 3 = $CHCl_3$, 4 = acetonitrile, 5 = 2-propanol, 6 = acetone, 7 = pyridine, 8 = DMSO, 9 = *o*-dichlorobenzene, 10 = ethylene glycol, 11 = hexafluoro-2-propanol) measured as the distance between the centroids of the spectral peaks at their full-width at three-quarters maximum, versus the strength of the solvent dielectric reaction field.

By plotting the steady-state Stokes shift as a function of the solvent dielectric, we can obtain the size of the change in charge distribution of the molecular system upon absorption of a photon. The Stokes shift is measured as the distance between the centroid of the absorption and fluorescence peaks at the full-width three-quarters maximum since this measure is more reproducible than the peak position. The Lippert−Mataga formula is the simplest way to relate the Stokes shift $\delta\nu$ of a dipolar molecule to the solvent dielectric properties:

$$\delta\nu = \frac{2(\mu_e - \mu_g)^2}{chR^3}\left[\frac{\epsilon_0 - 1}{2\epsilon_0 + 1}\frac{n^2 - 1}{2n^2 + 1}\right] \qquad (1)$$

where $\mu_{e,g}$ is the dipole moment of a given electronic state, R is the radius of a sphere containing the solute dipole, and ϵ_0 and n^2 are the static and optical dielectric constants. LD690 and LDS750 are both salts and exist in solution as cations, but since absorption of a photon results in a redistribution of charge on the molecule and not a change in the amount of charge, we (along with other workers) model the energetics as an effective dipole change. Since the energetics of solvation depends only on the total quantity $\Delta\mu^2/R^3$, we use this quantity as the measure of the solute−solvent coupling. Figure 3a shows this plot for

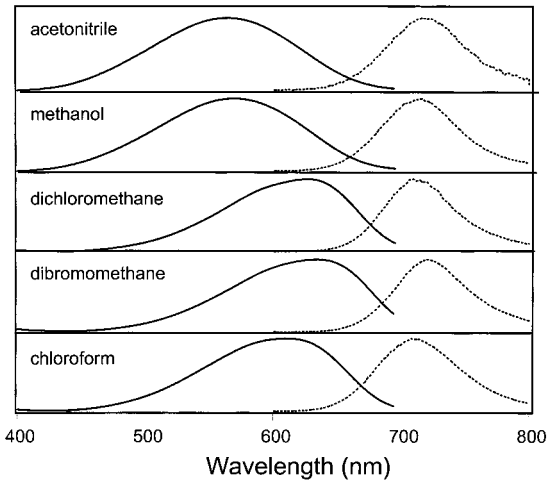

Figure 4. Absorption (solid lines) and fluorescence (dashed lines) spectra of LDS750 in various solvents.

LD690 in a series of *n*-alcohols, and we extract a slope of 2718 cm^{-1} from a linear least-squares fit to the data. Fits of the Stokes shift data to other solvent parameters, such as the solvent polarity function E_N^T,[30,31] do not result in a plot with less scatter than that shown in Figure 3a.

We have also measured the absorption and fluorescence of LD690 in other solvents, and these data is summarized in Figure 3b, which plots the Stokes shift against the dielectric reaction field in other solvents. In no other solvents, including the hydrogen-bonding solvents ethylene glycol and hexafluoro-2-propanol (HFIP), do we see the double-peaked fluorescence spectrum seen in the alcohols. In all solvents the shape of the fluorescence spectrum is similar to that observed in methanol, close to a mirror image of the absorption. The slope of a linear least-squares fit to these data is 1798 cm^{-1}, considerably less than that obtained in the *n*-alcohols. However, there is also considerably more scatter in the data, and some solvents, notably the halomethanes (CH_2Cl_2 CH_2Br_2, and $CHCl_3$), do not follow the trend predicted by eq 1 even qualitatively. The HFIP data are also inconsistent with the data in the other alcohols, exhibiting a relatively small Stokes shift despite its high polarity. It is clear that the simple dielectric description embodied in eq 1 is not sufficient to accurately describe the behavior of LD690 in all solvents, although it seems to work very well in a limited class of solvents, notably the *n*-alcohols. We will return to this point later in the Discussion.

Figure 4 shows the measured absorption and fluorescence spectra for LDS750 in several solvents. In these solvents the fluorescence spectrum is about half as broad as the absorption and, like that of LD690, does not shift appreciably from solvent to solvent. The absorption spectrum, while always broad and featureless, does shift, especially in the halomethane solvents. The absorption's 50 nm shift and shape change in these solvents indicates a significant change in the solvation and energetics. Figure 5 shows a plot of the Stokes shift versus the dielectric reaction field strength for these solvents and the *n*-alcohols ($n = 1-4$), giving a slope of 9481 cm^{-1}. In Figure 5 we see that the trend in the halomethane data is again the reverse of that predicted by eq 1. These data indicate that the parameter $\Delta\mu^2/R^3$ is at least 3 times larger for LDS750 than for LD690. In other words, the electrostatic perturbation due to photoexcitation and the consequent rearrangement of charge is considerably larger in LDS750 than in LD690.

To determine the underlying vibronic structure of the steady-state absorption and fluorescence spectra, we turn to resonance

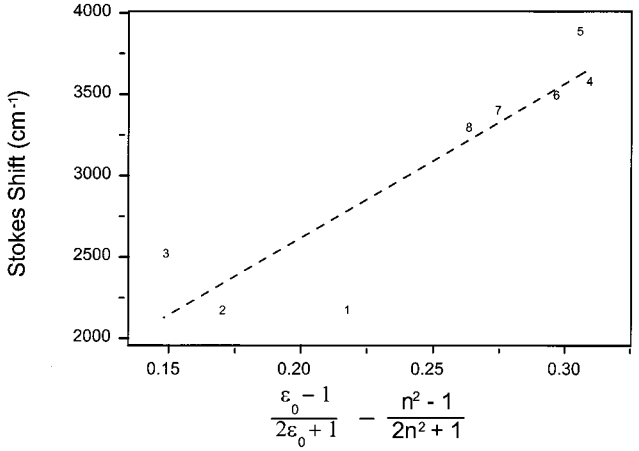

Figure 5. Plot of the Stokes shift of LDS750 in various solvents (1 = CH_2Cl_2, 2 = CH_2Br_2, 3 = $CHCl_3$, 4 methanol, 5 = acetonitrile, 6 = ethanol, 7 = *n*-propanol, 8 = *n*-butanol[32]) measured as the distance between the centroids of the spectral peaks at their full-width at three-quarters maximum, versus the strength of the solvent dielectric reaction field.

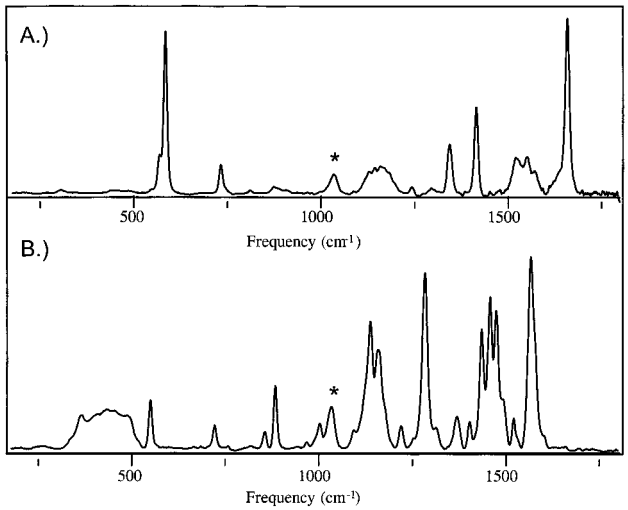

Figure 6. Resonance Raman spectrum of (A) LD690 in methanol and (B) LDS750 in methanol.

Raman, which is sensitive to vibrations that are directly coupled to the initial optical excitation.[33] The resonance Raman spectrum of LD690 in methanol is shown in Figure 6a. The peak at about 1033 cm^{-1} is a methanol solvent peak and is marked by an asterisk. LD690's spectrum is dominated by a single peak at 586 cm^{-1}, which we surmise to be an in-plane ring distortion by comparing its frequency to those observed in analogous compounds. Measurements were also performed on LD690 in CH_2Cl_2 and $CHCl_3$ as well as in ethylene glycol. The spectra in all these solvents are very similar. Minor changes are observed in $CHCl_3$ where the broad grouping of peaks around 1150 cm^{-1} appears to coalesce into a single peak, and in methanol, which is the only solvent where the peak at 880 cm^{-1} appears. We have also performed resonant Raman measurements on LDS750 in methanol, and these data are shown in Figure 6b. Here we see a much greater density of modes, especially at higher frequencies, and many of the peaks are broad and overlapping. Unlike LD690, LDS750 has no single dominant vibrational mode. The most remarkable thing about this spectrum, aside from its congestion, is the large, shapeless mass of peaks centered near 400 cm^{-1}. This feature is quite similar to a feature seen in the spectrum of neat methanol but is greatly enhanced relative to the methanol peak at 1033 cm^{-1}. Note that these

TABLE 1: Frequencies ω (in cm^{-1}) and Dimensionless Displacements D for the Observed Lines in the Resonance Raman Spectra of LD690 and LDS750 in Methanol

LD690 in methanol		LDS750 in methanol	
ω	D	ω	D
306	0.272	366	0.645
570	0.432	399	0.339
586	0.800	426	0.537
733	0.288	460	0.561
812	0.068	492	0.396
880	0.160	550	0.288
1130	0.192	721	0.159
1144	0.216	856	0.123
1176	0.144	884	0.204
1242	0.248	968	0.057
1345	0.080	988	0.069
1364	0.232	1002	0.129
1416	0.264	1094	0.108
1525	0.280	1131	0.303
1552	0.192	1137	0.156
1572	0.184	1158	0.237
1651	0.368	1175	0.159
1660	0.184	1220	0.108
		1283	0.300
		1310	0.105
		1368	0.129
		1404	0.093
		1434	0.204
		1456	0.204
		1473	0.192
		1490	0.147
		1520	0.084
		1564	0.159
		1570	0.249

low-frequency modes are barely discernible in the spectrum in Figure 6a. This apparent enhancement of the solvent modes due to the presence of the LDS750 solute, along with the smaller solvent-induced changes in the spectrum of LD690, suggest that the solvent and solute may be vibrationally coupled.

A tabulation of the D's and the ω's of both LD690 and LDS750 in methanol is given in Table 1. The vibrational frequency is obtained from a calibration of the spectrometer using a sample with a known spectrum, while the relative dimensionless displacement D is determined by integrating the area under individual peaks, after subtracting the neat solvent contribution, and using the relation[34]

$$I(\omega) \propto D^2\omega^2 \tag{2}$$

Equation 2 holds in the limit of fast electronic dephasing and reflects the fact that higher frequency vibrations can make larger excursions within the short temporal window defined by the electronic dephasing time. For example, when this enhancement of the high-frequency modes is taken into account for LD690, one finds that D_{1662} is approximately one-third of D_{586} even though the experimentally measured peaks are the same height. These relative displacements are then scaled by a constant factor in order to fit the measured width and shape of the absorption spectrum, which is calculated using the information from Table 1 and the dephasing parameters obtained from the femtosecond photon echo experiments described below. Analyses of LD690 in different solvents ($CHCl_3$, CH_2Cl_2, ethylene glycol) gave virtually identical spectra and thus identical ω's and D's. This procedure most likely results in an overestimation of the displacements D, given that the Stokes shift predicted from vibrational relaxation alone, using the values in Table 1, is 1421 cm^{-1}. This is almost twice that observed experimentally in methanol, 715 cm^{-1}, which is due both to vibrational and solvent relaxation.

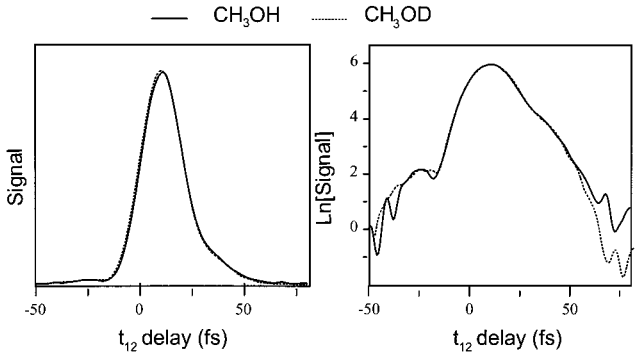

Figure 7. Experimental 3PPE signal for LD690 in CH_3OH (solid lines) and CH_3OD (dashed lines) with $t_{13} = 120$ fs.

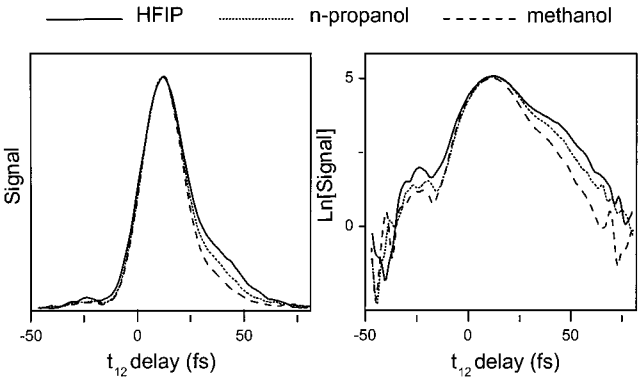

Figure 8. Experimental 3PPE signal for LD690 in hexafluoro-2-propanol (solid lines), *n*-propanol (short dashed lines), and methanol (long dashed lines) with $t_{13} = 120$ fs.

B. Time Domain Measurements. In previous work,[15] we measured the 3PPE signal in a series of *n*-alcohols. The slowing down in the decay with increasing alcohol chain length was attributed to a decrease in the density of the polar −OH groups around the solute. To further examine the role of the −OH motion on the ultrafast solvation in alcohols, we compare 3PPE data in regular and deuterated methanol. The 3PPE signals of LD690 in CH_3OH and CH_3OD are shown in Figure 7, along with their natural logarithms to show the signal at long delays. The experiment shows scans t_{12} with $t_{13} = 120$ fs, taking advantage of the mode suppression technique to obtain the most clearly resolved signal. There is no discernible difference between the methanol and deuterated methanol signals. Recent theory has suggested that solvation in alcohols proceeds via librational motion of the −OH group, which at short times can be approximated as inertial rotation. Substitution of a deuterium for a hydrogen increases the reduced mass of this functional group and thus reduces the libration frequency, resulting in slower solvation. No slow solvation in deuterated methanol is resolved in these data, although deuterium isotope effects have been observed in other experiments designed to probe ultrafast solvation.[35,36] In the alcohol series, systematic variations do exist, although the changes are not dramatic. Besides our previous data in the *n*-alcohols, Figure 8 shows the 3PPE signals in hexafluoro-2-propanol (HFIP), *n*-propanol, and methanol, scanning t_{12} with $t_{13} = 120$ fs. The polarization decay slows as we go from the smaller to larger alcohol molecules.

While the alcohol solvents are large and flexible molecules, the halomethane solvents should be well approximated as rigid dipoles and solvation would be dominated by rotational motion. Figure 9 shows the 3PPE signals in the three halomethane solvents with varying moments of inertia. There is very little change in the 3PPE decay, measured with $t_{12} = 120$ fs. The

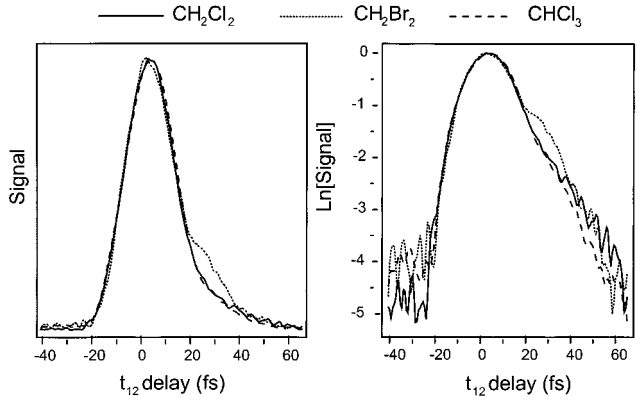

Figure 9. Experimental 3PPE signal for LD690 in CH_2Cl_2 (solid lines), CH_2Br_2 (short dashed lines), and $CHCl_3$ (long dashed lines) with $t_{13} = 120$ fs.

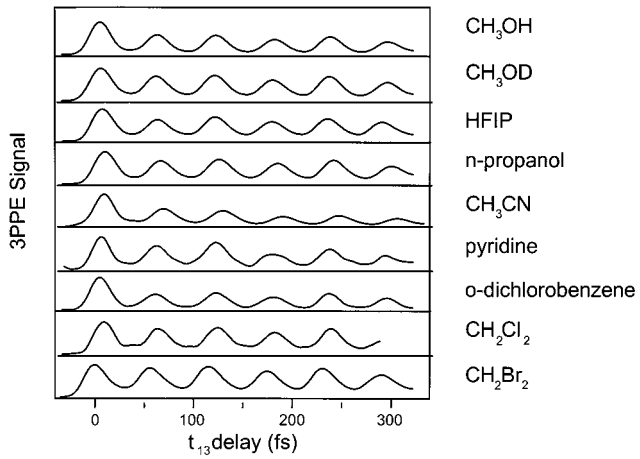

Figure 10. Experimental 3PPE signal of LD690 in various solvents, $t_{12} = 20$ fs and scanning t_{13}.

slight bulge at $t_{12} = 30$ fs in the CH_2Br_2 signal is reproducible and suggests that the heavier bromines slow the decay down somewhat. The CH_2Cl_2 and $CHCl_3$ decays are identical to within the experimental error, despite large differences in mass and rotational moment of inertia.

3PPE experiments were performed on LD690 in several other room temperature liquids, including acetone, DMSO, acetonitrile, pyridine, and *o*-dichlorobenzene. Although the detailed shapes and decay times of the signals differ slightly from solvent to solvent, all the polarization decays are on the time scale of 60 fs.

Scanning t_{13} with $t_{12} = 20$ fs we see that the population signals from the various solvents shown in Figure 10 are very similar. As discussed above, this signal is sensitive to the ultrafast solvation correlation time τ_c. With the exception of acetonitrile, these scans show no sign of the tell tale decay at $t_{13} > t_{12}$ that would indicate we are resolving a nonzero correlation time. The conclusion is that τ_c must be fairly short, and a more complete discussion of this point will be given below when we present calculations to model these data.

The 3PPE signal in LDS750 is qualitatively different from that of LD690. The first difference is that LDS750 has no single dominant vibrational mode on which we can use the mode suppression technique. Figure 11 shows the population scan with $t_{12} = 0$ for LDS750 in the four solvents used (methanol, acetonitrile, CH_2Cl_2, and CH_2Br_2). The amplitude of the fast decay of the population signal in acetonitrile decreases in methanol and is smaller still in CH_2Cl_2 and CH_2Br_2. The decay

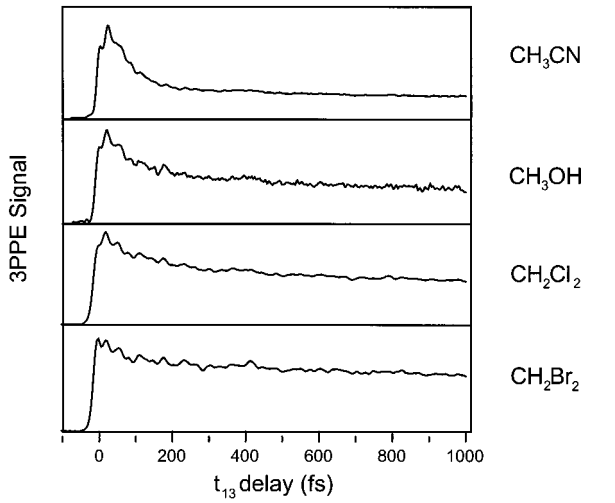

Figure 11. Experimental 3PPE signal of LDS750 in various solvents, $t_{12} = 0$ fs and scanning t_{13}.

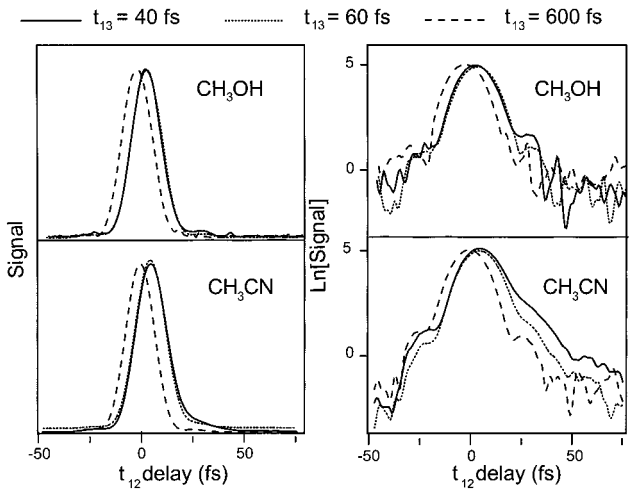

Figure 12. Experimental 3PPE signals for LDS750 in methanol and acetonitrile for t_{13} delays of 40, 60, and 600 fs.

of the polarization is also solvent-dependent. Figure 12 compares the polarization decay in methanol with that in acetonitrile as a function of t_{13}. In methanol, the decay is faster than our temporal resolution, and the signal mainly reflects the features of the pulse shape, while the acetonitrile data do exhibit a resolved decay, which disappears as t_{13} is increased. In both solvents, LDS750 appears to be subject to a very rapid, solvent-independent spectral diffusion process, unlike LD690. The observed signal depends strongly on the value of t_{13}, but not in the periodic manner observed in LD690 due to the 586 cm^{-1} mode. For LDS750, the apparent decay rate only decreases as t_{13} increases, and this decrease happens more quickly in methanol and the halomethanes than in acetonitrile.

C. Calculations of the 3PPE Signals. To analyze the 3PPE data, we simulate the experimentally measured signals by numerically evaluating the time-dependent nonlinear optical polarization generated by our ultrashort pulses.[15,37,38] The 3PPE signal detected in the phase-matched $-\mathbf{k}_1 + \mathbf{k}_2 + \mathbf{k}_3$ direction as a function of the relative pulse delays t_{12} and t_{13} is

$$S(t_{12},t_{13}) = \int_{-\infty}^{+\infty} dt\, |P^{(3)}(t)|^2 \qquad (3)$$

To obtain $P^{(3)}(t)$, we must numerically integrate the four time correlation functions that result from solving the time-dependent

Louiville equation perturbatively to third order:

$$P^{(3)}(t) = \left(\frac{i}{\hbar}\right)^3 \int_{-\infty}^{t} dt' \int_{-\infty}^{t'} dt'' \int_{-\infty}^{t''} dt''' \times E(t')\,E(t'')\,E(t''') x \sum_{i=1}^{4} R_i(t-t', t'-t'', t''-t''') \quad (4)$$

where R_i can be written as the product of harmonic oscillator linear response functions,[37] for instance,

$$R_1(t_1,t_2,t_3) = \exp[g(t_1) + g^*(t_2) + g^*(t_1+t_2+t_3) - g(t_1+t_2) - g^*(t_2+t_3)] \quad (5)$$

The line shape function $g(t)$ is evaluated for undamped harmonic oscillators for the case of intramolecular vibrational modes and as a stochastic broadening function to take intermolecular solvent effects into account,

$$g_{\text{intra}}(t) = \frac{D^2}{2}[(\bar{n}+1)(e^{-i\omega t}-1) + \bar{n}(e^{i\omega t}-1)] \quad (6)$$

$$g_{\text{inter}}(t) = i\lambda \int_0^t dt'\, M(t') + \Delta^2 \int_0^t dt' \int_0^{t'} dt''\, M(t'') \quad (7)$$

The electric field $E(t)$ is the Fourier transform of the magnitude of experimentally measured pulse power spectrum shown in Figure 1 (i.e., we assume the pulse to be transform-limited). The intramolecular vibrational frequencies and displacements are from Table 1. Note that eq 5 assumes that the intramolecular oscillators are undamped, i.e., intramolecular vibrational relaxation and vibrational dephasing are neglected. Ultrafast dissipation processes are taken into account by the solvation correlation function $M(t)$. The total $M(t)$ in eq 6 is divided into two parts: a stationary component ($\tau_c \rightarrow \infty$), which results in a Gaussian inhomogeneous broadening, and a component that undergoes a Gaussian decay to model the fast (homogeneous) dephasing. The choice of a Gaussian form for the fast decay is dictated by theoretical results which imply that such a form is the best description of the initial component of $M(t)$.[18,19] In reality, our data are not of sufficiently high resolution to distinguish between a Gaussian as opposed to an exponential or sech^2 form for $M(t)$ with similar decay times. The main goal of these experiments is to determine the time scale for the decay of $M(t)$, not its exact functional form.

The fact that the fluorescence data in Figure 2 implies the existence of two different excited-state conformers brings into question the validity of the simple two electronic-state model used to analyze the LD690 data. Since the fluorescence spectrum is independent of excitation wavelength, we know the fluorescence originates from a totally relaxed excited state, formed picoseconds to nanoseconds after the absorption of a photon. In our femtosecond experiments, we are only concerned with dynamics within at most the first picosecond after excitation. The two fluorescing species are likely formed long after the initial excitation to a single state and should have little or no bearing on the interpretation of our short pulse experiments.

We do not attempt to use extract the actual correlation function itself from the raw data[8] due to the complexity of the multimode response. Rather, we vary the parameters of our calculation and try to obtain a calculated signal that matches the experimental data. We begin with the observed absorption spectrum and the polarization decay. To fit the data, we guess a value for τ_c and then tune the Δ parameter to get a polarization (t_{12}) decay that matches the experiment. This combination of Δ and τ_c determines the effective homogeneous dephasing, and the inhomogeneous broadening parameter σ is set by matching the calculated and measured absorption spectra. We have found that the femtosecond decay of the 3PPE polarization signal is largely insensitive to small changes (10−30%) in σ, while the absorption spectrum changes significantly. Last, we check that the population dynamics are well described by these parameters, especially the decay of the t_{13} signal for a finite value of t_{12}. An example of this approach, applied to LD690, is outlined in Figure 13, which shows that even though a variety of parameters can adequately model the absorption spectrum and polarization decay, setting $t_{12} = 20$ fs and scanning t_{13} still provide a constraint on the value of τ_c. Note that when $\tau_c = 300$ fs, it is impossible to simultaneously model even just the polarization decay and the absorption spectrum. The parameters used for the calculations in Figure 13 are given in Table 2. To expedite the calculations used to generate Figure 13, 2 fs Gaussian pulses were used, rather than the experimentally measured $E(t)$'s used for all the other calculations in this work.

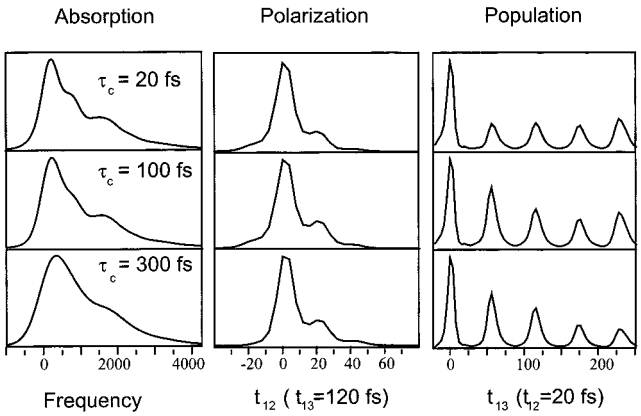

Figure 13. Model calculations for LD690 with various correlation times. The molecular parameters are summarized in Tables 1 and 2, and the electric fields used in the calculations are 2 fs Gaussian pulses.

TABLE 2: Dephasing Parameters Used for the Calculated Signals in Figure 13[a]

2λ (ps^{-1})	Δ (ps^{-1})	τ_c (fs)	σ (cm^{-1})
7.72	43.3	20	160
5.84	43.3	100	160
17.7	65.9	300	0

[a] 2λ is the Stokes shift, Δ is the magnitude of the energy fluctuations, τ_c is the correlation time of $M(t)$, and σ is the standard deviation of the Gaussian inhomogeneous broadening function.

Using the approach outlined above, we find that $M(t)$ decays in less than 100 fs in all the solvents examined. As can be seen from the experimental data in Figures 7−9, the polarization decay of LD690 does not vary dramatically from solvent to solvent, although the relatively small changes observed are reproducible. We will take two solvents, acetonitrile and CH_2Cl_2, as representative cases. Figure 14 shows the experimental and calculated 3PPE polarization decay for LD690 in acetonitrile, with $t_{13} = 120$ fs and scanning t_{12}. Figure 15 shows the measured absorption spectrum and the one calculated using the same parameters used in Figure 14. Finally, the calculated and measured 3PPE signal with $t_{12} = 20$ fs and scanning t_{13} is shown in Figure 16. The calculated signal has been multiplied by a factor of 0.65 so that the calculated and measured signals for the region $t_{13} > t_{12}$ overlap. The absolute size of this signal is very sensitive to the polarization decay seen in Figure 14, which we have not perfectly fit, but the form of the signal for $t_{13} > t_{12}$ is sensitive only to τ_c. Note that the observed decay in the oscillations in Figure 16 necessitates the use of a fairly large

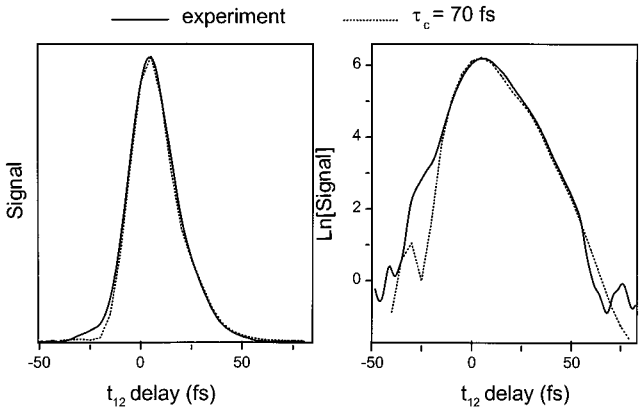

Figure 14. Experimental (solid lines) and calculated (dashed lines) 3PPE signals (t_{13} =120 fs and scanning t_{12}) for LD690 in acetonitrile.

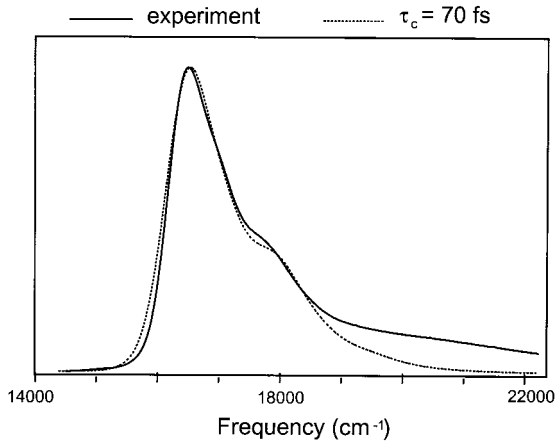

Figure 15. Experimental (solid line) and calculated (dashed line) absorption spectra for LD690 in acetonitrile.

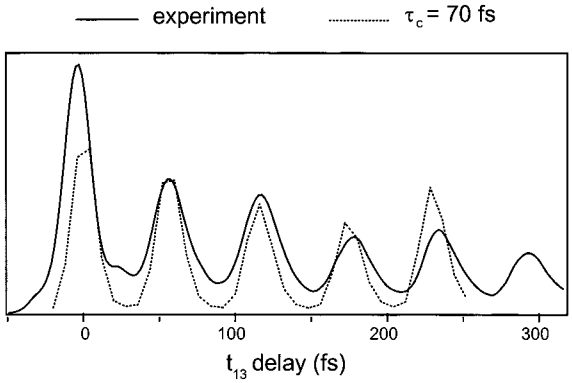

Figure 16. Experimental (solid line) and calculated (dashed line) 3PPE signals (t_{12} = 20 fs and scanning t_{13}) for LD690 in acetonitrile.

TABLE 3: Dephasing Parameters Used for the Calculated Signals for LD690 in Figures 14−18

solvent	2λ (ps^{-1})	Δ (ps^{-1})	τ_c (fs)	σ (cm^{-1})
CH_3CN	4.71	33.9	70	275
CH_2Cl_2	3.77	43.3	20	170

value for τ_c of 70 fs. This value for the decay time of $M(t)$ for LDS750 in acetonitrile is consistent with those from previous time-resolved measurements.[7,39] The calculations show good agreement with the data, and the parameters are summarized in Table 3, along with those from the dichloromethane data discussed below.

It turns out that acetonitrile is the exception. As can be seen in Figure 10, it is the only solvent for which there is a noticeable

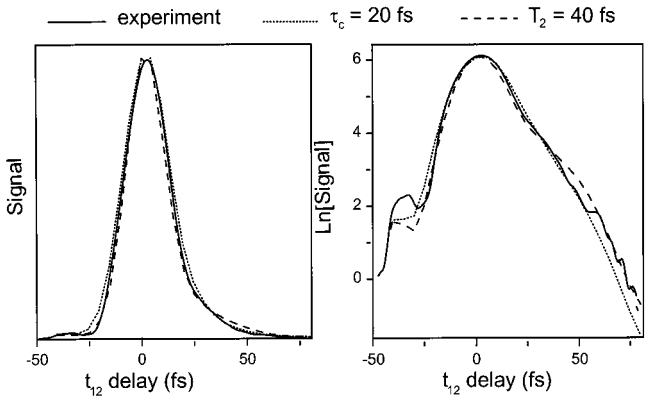

Figure 17. Experimental (solid lines) and calculated (dashed lines) 3PPE signals (t_{13} = 120 fs and scanning t_{12}) for LD690 in dichloromethane.

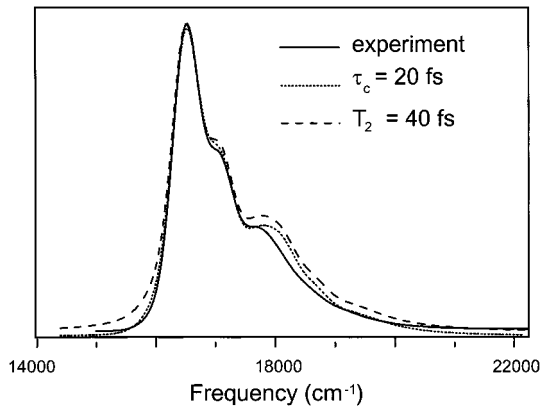

Figure 18. Experimental (solid line) and calculated (dashed lines) absorption spectra for LD690 in dichloromethane.

decay of the t_{12} = 20 fs, scanning t_{13} signal. All the other solvents studied appear to be in the fast modulation regime, with a significantly shorter correlation time than that observed in acetonitrile. In fact, most of the time domain data are consistent with a purely Markovian description of the dephasing. The necessity of achieving a fully self-consistent description of all the data, both time and frequency domain, is what causes us to model the data in terms of a non-Markovian process. We illustrate this for the case of LD690 in CH_2Cl_2, which has a considerably sharper absorption spectrum than that of acetonitrile and thus might be expected to show slower dephasing. Figure 17, which plots the experimental and calculated 3PPE signals for t_{13} = 120 fs, shows that this is not the case. In this figure we plot signals calculated using a finite τ_c of 20 fs and also a conventional T_2 of 40 fs. In the Markovian limit, T_2 is proportional to $^2\tau_c$, which is 47 fs for the CH_2Cl_2 values of Δ and τ_c in Table 3. Either approach gives an acceptable representation of the polarization (t_{12}) data, and this is also the case for the population (t_{13}) data. The data that show that the non-Markovian calculation are the truer representation of the dephasing dynamics in the linear absorption. This is plotted in Figure 18, along with the Markovian and non-Markovian calculations. We see that the Markovian calculation overestimates the wing on the red edge of the absorption spectrum, while the τ_c = 20 fs calculation gives a much better fit to this region. This can be understood in the following way: in order to fit the 3PPE data, T_2 must be fairly short, and the Fourier transform of this fast exponential decay is a Lorentzian with substantial wings. This is why we see the long wing extending to the low-frequency side of the calculated absorption spectrum. The wings of the spectrum are sensitive to the very early time

behavior of the polarization decay, a region that we cannot access directly due to the finite length of our pulses. The introduction of a finite (albeit small) correlation time is enough to smooth out the early time behavior of the polarization and decrease the wings of the calculated spectra. If we had no time domain data, we could accomplish this by making T_2 longer and having a predominantly inhomogeneously broadened spectrum that would be more Gaussian with smaller wings. It is the combination of time and frequency domain data that allows us to claim that the femtosecond dephasing of LD690 in dichloromethane is non-Markovian. The analysis of the data in all the other solvents has not been done but would proceed in the same way to the same general conclusions. It is worth noting that although the absorption spectra in Figure 2 show considerable variation in width, this variation appears to be largely the result of changes in the slower solvation processes, which are treated as inhomogeneous broadening in the present work.

We now turn to the LDS750 data. Modeling the experimental data for LDS750 is problematic for several reasons. First, the absorption spectrum is extremely broad and without any discernible vibrational structure, which makes it difficult to determine the scaling of the displacements determined from the resonance Raman data. Second, the time-domain signal is very close to pulse width limited, and in such cases the experimental signal is much more sensitive to experimental details such as the structure of the pulse spectrum. The mode suppression technique is not effective in this case because there is no single dominant vibrational mode and also because LDS750 undergoes a very rapid spectral diffusion process (see Figure 12) so that the fast dephasing information is lost on the time scale of a vibration. We did attempt to develop a complete multimode model for the dynamics, but the fits to the absorption spectrum and time-domain data were not nearly as good as in the case of LD690. However, it is possible to draw some qualitative conclusions about the solvation of LD690. First, from Figure 11, we can see that the magnitude of the population relaxation (which is due to the Stokes shift of the emission outside the window of the exciting pulse) decreases as we go from acetonitrile to CH_2Br_2. But although the acetonitrile data exhibit the largest population shift, it has the slowest polarization decay, as shown in Figure 12. Both the CH_2Cl_2 and CH_2Br_2 data are as fast as methanol, essentially pulse width limited. The amount of population relaxation observed in Figure 11 does not correlate well with the polarization dynamics, and we can estimate that the correlation times for LDS750 solvation are faster in methanol and the halomethanes than in acetonitrile.

Discussion

We now turn to the question of the microscopic origin of $M(t)$. One possibility is that our model for the intramolecular vibrational dynamics of the solute, while it is consistent with the resonance Raman and absorption spectra, is still incomplete. We have assumed that the excited state is a displaced replica of the ground state with no Dushinsky rotation or frequency changes. However, as noted above, our values for the excited-state displacements result in an excess vibrational Stokes shift that is not observed experimentally. Part of this discrepancy is likely due to the limited amount of resonance Raman data available—we only have spectra for a single wavelength, while ideally we would collect data at several wavelengths to obtain a Raman excitation profile. However, the assumption of undamped intramolecular oscillators may also be incorrect, and there may be significant intramode couplings and relaxation mechanisms that contribute to the sub-100 fs decay of the polarization.[40] This is especially a concern for LDS750, whose electronic transition is coupled to many more vibrational modes, both high and low frequency, which at the very least tend to obscure the solvation dynamics. Furthermore, transient absorption and emission experiments suggest that fast intramolecular relaxation in this molecule leads to a solvent-mediated isomerization.[41] LD690, on the other hand, seems to be much better behaved in terms of its excited-state dynamics, with the 586 cm^{-1} oscillations showing no sign of subpicosecond intramolecular relaxation in pump−probe and transient grating experiments, which have been successfully described by the present multimode model.[42] Although small, the variation in the ultrafast dephasing with solvent, especially in the *n*-alcohols,[15] demonstrates that even if the ultrafast dephasing is due to an intramolecular process, such a process must be mediated by the solvent. Finally, the femtosecond optical dephasing of LD690 also shows a strong temperature dependence,[43] which would not be expected if it was solely the result of a high-frequency vibration or a polarization free decay due to the multiplicity of vibrational modes.

Thus, the experimental evidence shows that the optical dephasing in both is due, at least in part, to intermolecular interactions with the solvent molecules. We will discuss two models for this interaction in the context of our results.

Molecular dynamics simulations have suggested that the initial solvation is the result of "inertial" motion of the solvent dipoles. In principle, this ultrafast motion may be either vibrational or rotational, but since most molecular dynamics simulations assume rigid molecules, rotational motion is studied most often. All simulations predict a two-component decay of $M(t)$, a fast inertial decay that occurs on the time scale of approximately 100 fs, and a slower "diffusive" decay that occurs on a time scale of picoseconds to nanoseconds. Theoretical work and simulations predict that the inertial component of the solvation correlation function, written here as $M_i(t)$, should have a Gaussian form[18,19]

$$M_i(t) = \langle U(0)\, U(t)\rangle_c \cong \Delta^2 \exp\left[-\frac{1}{2}\omega_S{}^2 t^2\right] \qquad (8)$$

where $U = H_e - H_g$ is the time-varying energy gap between the ground and excited electronic states. Maroncelli and coworkers have derived a simple expression for the solvation frequency ω_S, in terms of the rotational properties of the solvent molecules:[20,44]

$$\omega_S{}^2 = \left[\frac{4\pi\rho\mu^2}{3kT}\right]\left[\frac{\epsilon_0}{\epsilon_0 - 1}\right]\langle\omega_R{}^2\rangle \qquad (9)$$

where ρ is the number density of the solvent molecules, and μ is the solvent dipole. In this model, ω_S, the solvation frequency, is directly related to ω_R, the average rotational frequency of a free solvent molecule weighted by its dipole moment elements. Both the time scale and the magnitude of the inertial component is related to the dipole density of the solvent, which depends on both the static dielectric constant ϵ_0 and the solvent density and molecular dipole moments. A detailed numerical comparison of our data with the predictions of this theory is beyond the scope of this paper. Instead, we compare qualitative trends in the data with those predicted by the theory. Examination of eq 8 and calculations by Maroncelli and co-workers[44] show that the decay rate and relative magnitude of the inertial component should decrease with decreasing solvent dielectric strength. While previous data in alcohols have shown that the size of the inertial component does seem to decrease as the alcohol size

increases (and ϵ_0 and ρ decrease), no change in the time scale of the inertial component was observed. Instead, as discussed in the Results, the correlation time τ_c for LD690 remained remarkably constant at 20 fs throughout the alcohols, halomethanes, and a variety of other solvents with very different properties. If we compare the acetonitrile data ($\tau_c = 70$ fs) with the methanol data ($\tau_c = 20$ fs), the decay of $M(t)$ speeds up by roughly the amount predicted by simulations.[22,23,45,46] This is expected due to the simple fact that the OH group librates faster than the heavier acetonitrile rotates. If we now compare the acetonitrile data with that from the chlorinated methanes, we find that again the trend predicted by the simple inertial rotational motion does not hold. The heavier, less polar halomethanes would be expected to have a slower inertial response, with a smaller magnitude, than acetonitrile.[44] However, the best modeling of the LD690 data leads to a faster inertial decay with a magnitude comparable to that of acetonitrile. Finally, the lack of an isotope effect in the dephasing dynamics of LD690 in methanol shown in Figure 7 also suggests that the ultrafast solvation involves more than simple librational motion of the hydroxyl group. However, it is possible that the change due to deuteration is beyond the resolution of this experiment, since the data could probably be fit fairly well with a correlation time of 30 fs $\approx \sqrt{2}\tau_c$ in regular methanol.

Recently, solvation theories based on a knowledge of the frequency-dependent solvent dielectric dispersion $\epsilon(\omega)$ in combination with an effective solute cavity[21−23] have been shown to result in good agreement with experimentally measured time-dependent Stokes shifts of Coumarin molecules in several solvents, including water, acetonitrile, and methanol. By taking the high-frequency component of the dielectric response into account, these calculations can even reproduce the sub-100 fs "inertial" component of the decay. This theoretical approach is attractive because it does not rely on the somewhat arbitrary definition of multiple Brownian oscillators of undetermined origin but rather allows the optical dynamics to be calculated directly from a knowledge of the bulk solvent properties and the size and shape of the solute molecule. However, the success of these theories raises the question as to whether molecular-level interactions between solvent and solute molecules play any role in the solvation process.

The data in this paper do suggest that such molecular-level interactions will have to be addressed in order to explain various aspects of solvation. The Stokes shift data in Figures 3 and 5 show that while the dielectric continuum picture works well for some classes of solvents, notably the *n*-alcohols, it does not describe the behavior of LD690 or LDS750 across different families of solvents. This is especially the case for the halomethanes and HFIP, where the Stokes shift trend is the opposite of that predicted by the Lippert−Mataga formula. The fact that the absorption spectrum of LDS750 changes shape so dramatically in CH_2Cl_2 and CH_2Br_2 as opposed to methanol and acetonitrile, and also the existence of two fluorescent isomers of LD690 in the larger *n*-alcohols, are further evidence that treating the solvent as a bulk dielectric medium is insufficient to explain the steady-state spectral properties of these solutes. Certainly the simplest picture of dielectric solvation of a point dipole in a spherical cavity is insufficient to explain the steady-state spectroscopy of LD690 and LDS750.

In addition to the analysis of the steady-state absorption/fluorescence data, the changes observed in the resonance Raman spectra of the two molecules also suggest that the solvent is interacting with the solute molecules on a more microscopic level. The enhancement of low-frequency solvent modes in the LDS750 resonance Raman spectrum, along with the small solvent-dependent changes observed for LD690, provide evidence that the solvent−solute interactions are strong enough to perturb the ground-state vibrational structure, an effect that dielectric continuum theory cannot predict.

The fast time scales observed in this work are consistent with the predictions of the dielectric approach, as is the trend in τ_c from acetonitrile to methanol.[21] High-frequency dielectric data are not available for many of the solvents used in this work, and whether this theory would predict a definite trend for the series of halomethanes and *n*-alcohols is an open question. There is no discernible effect of deuteration on the dynamics of LD690 in methanol, despite the effect this should have on the high-frequency region of $\epsilon(\omega)$, but as stated above, it is not clear that we can extract the expected change in $M(t)$ from our data. It may be that the dielectric approach will yield a satisfactory description of the dephasing once a realistic model of the solute is used. The Lippert−Mataga formula is the simplest possible description of the Stokes shift in terms of the solvent dielectric properties and has been improved upon by many workers using more molecular models for the solute and solvent.[47−49] Recent work by Fleming and co-workers has demonstrated how different models of the solvent response can lead to a better description of 3PPE results,[50] and work by Chandler and co-workers has shown how to incorporate a complex solute molecule and its charge distribution into continuum response theories.[23]

One possible difficulty for all theories based on bulk solvent properties is that those theories fail to take the molecular level interactions into account. Such interactions are known to be important in influencing the chemical reactivity of organic molecules in solution,[30] and recent experiments on Coumarin 102 in chloroform have suggested that the breaking of an intermolecular site-specific hydrogen bond plays a role in the earliest solvation dynamics.[51] Hydrogen bonding interactions have been implicated in nonsystematic deviations from dielectric continuum behavior on picosecond time scales as well.[52] LD690 is a cationic dye molecule, and it would be expected to be solvated preferentially by the electronegative oxygen atoms of the methanol molecules. If this were the case, the atomic level interactions between the oxygen atoms and the positively charged region of the molecule would be less sensitive to deuteration. On the other hand, such interactions would be sensitive to the packing of the electronegative oxygens, which depends on the alcohol chain length (as in the case of the *n*-alcohols), and on the net charge of the oxygen, which would be affected by halogen substitution on the alcohol (as in the case of HFIP). Similarly, atomic level interactions also provide an explanation as to why the 3PPE signals for LD690 in dichloromethane and chloroform are identical. These solvents are very different in terms of their bulk properties, but at the molecular level they may look the same to an LD690 molecule, especially if there are specific interactions between the chlorine atoms and LD690 that lead to the formation of a solvent−solute complex. In this picture of ultrafast solvation, the intramolecular dynamics are indirectly coupled to the solvent through specific interactions, like hydrogen bonds. While this work presents no direct proof of this hypothesis, it does help to explain the observed trends (or lack thereof) in various solvents.

Conclusion

We have shown that the electronic dephasing of LD690 in room-temperature liquids is non-Markovian, but with a very short correlation time. To prove that a simple T_2 is insufficient

to explain the data, we analyze both the time domain (3PPE) and frequency domain data (absorption, fluorescence, and resonance Raman) to obtain a self-consistent model that explains the spectroscopy of LD690. It should be emphasized that we did not begin by assuming that the dynamics must be non-Markovian and then modifying the parameters of a specific model to fit the time-resolved data, but rather by trying to model the data with the least possible number of parameters, either two (T_2 and σ) or three (τ_c, Δ, and σ). It should also be emphasized that a working knowledge of the resonance Raman spectrum is vital for obtaining quantitative values for the parameters in Tables 2 and 3. The LDS750 data show how any analysis of solvent influence on electronic dephasing must take the nature of the probe molecule into account and that dynamics observed in the population (t_{13}) part of the 3PPE experiment are not straightforwardly related to those observed in the polarization (t_{12}) part. The important point is that even at the simplest level, the observed dephasing depends critically on the solute molecule itself, and this can influence what type of experiment is most appropriate to probe solvation dynamics. Finally, we find that simple theories of solvation, such as treating the solvent molecules as inertial dipolar rotors or as a dielectric continuum, are insufficient to explain the observed trends for LD690. Whether more realistic models of the solutes, coupled with these theories based on bulk solvent properties, will be sufficient to model the solvation dynamics for any given solute molecule is unclear, although there has been progress in that direction. The possibility that the electronic dephasing of a molecule in solution is determined by specific chemical interactions between that molecule and specific solvent molecules, and not just by bulk solvent properties, is an intriguing one.

Acknowledgment. We thank Prof. R. A. Mathies for the use of his resonance Raman spectrometer, Prof. A. P. Alivisatos for the use of his fluorimeter, and Dr. R. W. Schoenlein for helpful discussions. This research was supported by the Department of Energy, Office of Basic Research.

References and Notes

(1) Villaeys, A. A.; Vallet, J. C.; Lin, S. H. *Phys. Rev. A* **1991**, *43*, 5030−5038.
(2) Myers, A. B.; Li, B. *J. Chem. Phys.* **1990**, *92*, 3310−3322.
(3) Yajima, T.; Souma, H. *Phys. Rev. A* **1978**, *17*, 309−323.
(4) Cong, P.; Yan, Y. J.; Deuel, H. P.; Simon, J. D. *J. Chem. Phys.* **1994**, *100*, 7855−7866.
(5) Ma, J.; Vanden bout, D.; Berg, M. *J. Chem. Phys.* **1995**, *103*, 9146−9160.
(6) Goldberg, S. Y.; Bart, E.; Meltsin, A.; Fainberg, B. D.; Huppert, D. *Chem. Phys.* **1994**, *183*, 217−233.
(7) Maroncelli, M.; Fleming, G. R. *J. Chem. Phys.* **1987**, *86*, 6221−6239.
(8) Bigot, J.-Y.; Portella, M. T.; Schoenlein, R. W.; Bardeen, C. J.; Migus, A.; Shank, C. V. *Phys. Rev. Lett.* **1991**, *66*, 1138−1141.
(9) Nibbering, E. T. J.; Wiersma, D. A.; Duppen, K.; *Phys. Rev. Lett.* **1991**, *66*, 2464−2467.
(10) Vohringer, P.; Arnett, D. C.; Westervelt, R. A.; Feldstein, M. J.; Scherer, N. F. *J. Chem. Phys.* **1995**, *102*, 4027−4036.
(11) Joo, T.; Jia, Y.; Yu, J.-Y.; Lang, M. J.; Fleming, G. R. *J. Chem. Phys.* **1996**, *104*, 6089−6108.
(12) Van der Zwan, G.; Hynes, J. T. *J. Phys. Chem.* **1985**, *89*, 4181−4188.
(13) Chandra, A.; Bagchi, B. *Chem. Phys. Lett.* **1990**, *165*, 93−99.
(14) De Boeij, W. P.; Pshenichnikov, M. S.; Wiersma, D. A. *J. Phys. Chem.* **1996**, *100*, 11806−11823.
(15) Bardeen, C. J.; Shank, C. V. *Chem. Phys. Lett.* **1994**, *226*, 310−316; *Chem. Phys. Lett.* **1993**, *203*, 535−539.
(16) Passino, S. A.; Nagasawa, Y.; Joo, T.; Fleming, G. R. *J. Phys. Chem. A* **1997**, *101*, 725−731.
(17) Lang, M. J.; Jordanides, X. J.; Song, X.; Fleming, G. R. *J. Chem. Phys.* **1999**, *110*, 5884−5892.
(18) Maroncelli, M.; Fleming, G. R. *J. Chem. Phys.* **1988**, *89*, 5044−5069.
(19) Carter, E. A.; Hynes, J. T. *J. Chem. Phys.* **1991**, *94*, 5961−5979.
(20) Maroncelli, M.; Kumar, V. P.; Papazyan, A. *J. Phys. Chem.* **1993**, *97*, 13−17.
(21) Hsu, C. P.; Song, X.; Marcus, R. A. *J. Phys. Chem. B* **1997**, *101*, 2546−2551.
(22) Hsu, C. P.; Georgievskii, Y.; Marcus, R. A. *J. Phys. Chem. A* **1998**, *102*, 2658−2666.
(23) Song, X.; Chandler, D. *J. Chem. Phys.* **1998**, *108*, 2594−2600.
(24) Weiner, A. M.; De Silvestri, S.; Ippen, E. P. *J. Opt. Soc. Am. B* **1985**, *2*, 654−661.
(25) De Boeij, W. P.; Pshenichnikov, M. S.; Wiersma, D. A. *Chem. Phys. Lett.* **1996**, *253*, 53−60.
(26) Schoenlein, R. W.; Mittleman, D. M.; Shiang, J. J.; Alivisatos, A. P.; Shank, C. V. *Phys. Rev. Lett.* **1993**, *70*, 1014−1017.
(27) De Boeij, W. P.; Pshenichnikov, M. S.; Wiersma, D. A. *J. Chem. Phys.* **1996**, *105*, 2953−2960.
(28) Yu, J.; Berg, M. *Chem. Phys. Lett.* **1993**, *208*, 315−320.
(29) Blanchard, G. J. *Chem. Phys.* **1989**, *138*, 365−375.
(30) *Solvents and Solvent Effects in Organic Chemistry*, 2nd ed.; Reichart, C., Ed.; VCH: Weinheim, Germany, 1998.
(31) Ravi, M.; Samanta, A.; Radhakrishnan, T. P. *J. Phys. Chem.* **1994**, *98*, 9133−9136.
(32) Castner, E. W.; Maroncelli, M.; Fleming, G. R. *J. Chem. Phys.* **1987**, *86*, 1090−1097.
(33) Lawless, M. K.; Mathies, R. A. *J. Chem. Phys.* **1992**, *96*, 8037−8045.
(34) Myers, A. B.; Harris, R. A.; Mathies, R. A. *J. Chem. Phys.* **1983**, *79*, 603−613.
(35) Reid, P. J.; Silva, C.; Barbara, P. F.; Karki, L.; Hupp, J. T. *J. Phys. Chem.* **1995**, *99*, 2609−2616.
(36) Emde, M. F.; Baltuska, A.; Kummrow, A.; Pshenichnikov, M. S.; Wiersma, D. A. *Phys. Rev. Lett.* **1998**, *80*, 4645−4648.
(37) Yan, Y. J.; Mukamel, S. *J. Chem. Phys.* **1988**, *89*, 5160−5176; *J. Chem. Phys.* **1991**, *94*, 179−190.
(38) Pollard, W. T.; Dexheimer, S. L.; Wang, Q.; Peteanu, L. A.; Shank, C. V.; Mathies, R. A. *J. Phys. Chem.* **1992**, *96*, 6147−6158.
(39) Rosenthal, S. J.; Xie, X.; Du, M.; Fleming, G. R. *J. Chem. Phys.* **1991**, *95*, 4715−4718.
(40) Book, L. D.; Scherer, N. F. *J. Chem. Phys.* **1999**, *111*, 792−795.
(41) Kovalenko, S. A.; Ernsting, N. P.; Ruthmann, J. *J. Chem. Phys.* **1997**, *106*, 3504−3511.
(42) Bardeen, C. J.; Wang, Q.; Shank, C. V. *J. Phys. Chem. A* **1998**, *102*, 2759−2766.
(43) Bardeen, C. J.; Cerullo, G.; Shank, C. V. *Chem. Phys. Lett.* **1997**, *280*, 127−133.
(44) Maroncelli, M.; Kumar, P. V.; Papazyan, A.; Horng, M. L.; Rosenthal, S. J.; Fleming, G. R. *AIP Conf. Proc.* **1994**, *298*, 310−323.
(45) Kumar, P. V.; Maroncelli, M. *J. Chem. Phys.* **1995**, *103*, 3038−3060.
(46) Fonseca, T.; Ladanyi, B. M. *J. Mol. Liq.* **1994**, *60*, 1−24.
(47) Matyushov, D. V.; Schmid, R.; Ladanyi, B. M. *J. Phys. Chem. B* **1997**, *101*, 1035−1050.
(48) Mertz, E. L.; German, E. D.; Kuznetsov, A. M. *Chem. Phys.* **1997**, *215*, 355−370.
(49) Bader, J. S.; Berne, B. J. *J. Chem. Phys.* **1996**, *104*, 1293−7308.
(50) Passino, S. A.; Nagasawa, Y.; Fleming, G. R. *J. Chem. Phys.* **1997**, *107*, 6094−6108.
(51) Chudoba, C.; Nibbering, E. T. J.; Elsaesser, T. *Phys. Rev. Lett.* **1998**, *81*, 3010−3013.
(52) Chapman, C. F.; Fee, R. S.; Maroncelli, M. *J. Phys. Chem.* **1995**, *99*, 4811−4819.